Sensors & Actuators: B. Chemical 320 (2020) 128432

Contents lists available at ScienceDirect

Sensors and Actuators B: Chemical

journal homepage: www.elsevier.com/locate/snb

Graphene based field-effect transistor biosensors functionalized using gas-phase synthesized gold nanoparticles

Eric Danielson[a,*], Vyankat A. Sontakke[b], Alexander J. Porkovich[a], Zhenwei Wang[a], Pawan Kumar[a], Zakaria Ziadi[a], Yohei Yokobayashi[b], Mukhles Sowwan[a]

[a] Nanoparticles by Design Unit, Okinawa Institute of Science and Technology (OIST) Graduate University, 1919-1 Tancha, Onna-Son, Okinawa, 904-0495, Japan
[b] Nucleic Acid Chemistry and Engineering Unit, Okinawa Institute of Science and Technology (OIST) Graduate University, 1919-1 Tancha, Onna-Son, Okinawa, 904-0495, Japan

ARTICLE INFO

Keywords:
Biosensor
Graphene
DNA
Gold nanoparticle functionalization
Gas-phase synthesis
Streptavidin

ABSTRACT

Research has focused on graphene for developing the next generation of label-free biosensors, capable of highly sensitive and specific detection of DNA or other biomolecules. The binding of charged analytes to the one-atom thick layer of graphene can greatly affect its electronic properties. However, graphene is highly chemically inert, thus surface functionalization through chemical treatment is typically necessary to immobilize receptors of the target biological analyte on the graphene. In this work, we use gas-phase synthesized gold nanoparticles (Au NPs) to functionalize and bind a DNA aptamer to the graphene surface. The graphene is employed in a liquid gated field-effect transistor (FET) configuration to detect the hybridization of the complementary DNA strand, as well as the protein streptavidin, at attomolar level (aM, 10^{-18} mol L^{-1}). The sensor shows a high dynamic detecting range from aM to picomolar (pM) levels (10^{-18} to 10^{-12} mol L^{-1}), can discriminate between a complementary strand and a single nucleotide polymorphism (SNP) containing strand, and achieves a detection limit as low as 15 aM. The high detection limit suggests that decorating biosensors with Au NPs synthesized from magnetron sputtering inert gas condensing technique is a promising method for biosensor functionalization, particularly for larger-area sensors that employ two-dimensional materials such as graphene.

1. Introduction

Field-effect transistors (FETs) have attracted widespread attention for their biosensing applications; particularly for DNA detection, as this capability is of fundamental interest in clinical diagnostics, environmental monitoring, forensics, and biomedical research [1–5]. DNA can also be developed into aptamers designed to bind to specific biomolecules for early disease detection [6,7]. Unlike traditional optical DNA sensing methods, FET based sensors do not require sophisticated photodetectors or extensive fluorescent labeling processes. This is because of FETs are solid state devices in which the channel conductance between the source and drain electrodes is controlled via the electrostatic gating effect from a third electrode [8]. In a biosensor FET, charged molecules may dope or apply a virtual gate bias upon binding to the semiconducting channel [4,9–11]. By functionalizing the FET with a specific biological recognition element, the binding of a target analyte produces a change in the channel conductance and a sensor response which is highly specific.

Graphene is an attractive nanomaterial in biosensors due to its excellent physical and chemical properties such as high carrier mobility and ease of functionalization [5]. Its one-atom thick nature, large surface area to volume ratio, and high conductivity allow graphene-based FETs (G-FETs) to be highly sensitive, with limits of detection (LoD) for nucleic acids in the high aM to low femtomolar range [7,11,12]. G-FETs have been employed as sensors for a wide variety of biological analytes, including small-molecule biomarkers, amino acids, enzymes, glucose, and nucleic acids [3,11,13–15]. In addition, two dimensional materials such as graphene are more compatible with standard planar technology and microfabrication at the wafer scale to produce arrays of multiple biosensors [16,17].

The selectivity of FET biosensors is typically defined by immobilizing receptor molecules on the device surface to uniquely bind to a targeted analyte, such as an antibody or a complementary DNA strand. As graphene is relatively inert, it must be chemically treated to generate active groups for the binding of biomolecules. Noble metal nanoparticles (NPs) deposited on graphene are widely used as binding sites, and have been shown to greatly enhance DNA detection sensitivity [11,15,18–20]. Gold NPs have been especially popular due to

* Corresponding author.
E-mail address: eric.danielson@oist.jp (E. Danielson).

https://doi.org/10.1016/j.snb.2020.128432
Received 13 March 2020; Received in revised form 23 May 2020; Accepted 6 June 2020
Available online 09 June 2020

their biocompatibility and well-known functionalization chemistry. Au has a high chemical affinity with thiol groups, enabling easy binding of thiol-terminated DNA to act as receptor molecules [10].

In this work, we successfully demonstrate the integration of Au NPs produced via a magnetron sputtering inert gas condensing technique in G-FET arrays for DNA sensing. This is the first demonstration of such NPs decorated G-FETs for bio-sensing applications and the method avoids the use of residual capping ligands or reactants present in solvent based methods that could interfere with the Au-thiol binding [21,22]. Gas-phase synthesis also allows for a high degree of control over the Au NP size and shape while ensuring a uniform coverage over a large area during deposition [23–25]. Combined with a scalable lamination procedure to transfer graphene grown using chemical vapor deposition (CVD) to Si:SiO_2 substates [16], this method can efficiently produce highly specific sensors with sensitivity down to the aM level at a large scale. A DNA aptamer is used to detect both a target DNA strand and streptavidin, a protein commonly used in biomedical research due to its high affinity for biotin. High selectivity is demonstrated by comparing the sensor response between fully complementary strands and those with a single nucleotide polymorphism (SNP).

2. Materials and methods

2.1. Graphene FET fabrication

Graphene was synthesized in a CVD system (Easytube 2000, FirstNano, USA) on a 30 μm thick commercial copper foil (Nilaco, Japan). The copper foil was sonicated in acetone and isopropyl alcohol (IPA) before CVD growth. The copper foil was first annealed for 1 h at 990 °C at 760 torr, with gas mixture of Ar and H_2 at flow rates of 4875 and 125 standard cubic centimeter per minute (sccm), respectively. The CVD growth step was then performed for 15 min at 1000 °C at 760 torr, with gas mixture of Ar, H_2, and CH_4 with flow rates of 4875, 125, and 2.5 sccm, respectively. The sample was subsequently cooled to room temperature under an Ar flow rate of 5000 sccm.

Graphene transfer from the copper foil to Si:SiO_2 substrates was performed using a Poly(vinyl alcohol) (PVA) lamination method [16]. PVA films (Cubic Coating) were initially rinsed in IPA and dried with N_2. Copper foil pieces with CVD grown graphene were placed in deionized (DI) water for 8 h to facilitate the intercalation of graphene from the Cu or Cu_2O surface [26]. After drying, the PVA film is laminated on top of the graphene covered copper foil at 110 °C and a speed of 15 mm/s using a commercial laminator (Meiko Shokai THS 330). The laminate was baked on a hot plate at 110 °C for 1 min to improve the PVA/graphene adhesion. Once the PVA film is peeled off the copper foil, it removes the graphene as well. The graphene on PVA can be transferred to the desired substrate using a second lamination step under the same conditions. Then the substrate is baked at 110 °C for 1 min, followed by peeling off the paper support of the PVA film while the sample is still on the hot plate. The PVA layer is removed by placing the substrate in room temperature DI water overnight, leaving a monolayer graphene layer on top of the target substrate.

Si:SiO_2 substrates covered with monolayer graphene were patterned into biosensor devices using photolithography and oxygen plasma etching. The Ti/Au contacts (5/50 nm) were deposited by e-beam evaporation and defined using photolithography. After lift-off of the metal contacts and cleaning in acetone and IPA, the graphene substrates were placed in 1-methyl-2-pyrrolidone (NMP) for 4 h to remove residual photoresist from the graphene surface.

A PDMS solution well was attached to the G-FET to protect the source and drain electrodes during liquid-gate measurements. Liquid PDMS was placed on the underside of a hollow PDMS cylinder, then cured at 90 °C for 1 h for good adhesion to the FET surface. The solution well enclosed 3 G-FETs, each with an area of 1 mm^2. A schematic of a completed enclosed Au NP decorated G-FET is shown in Fig. 1.

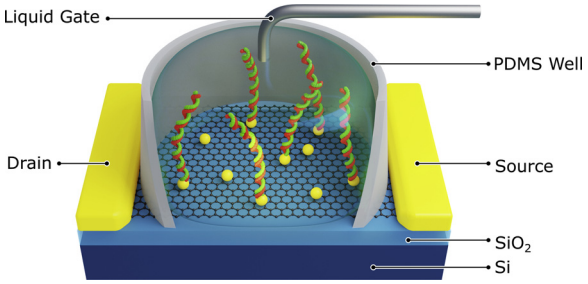

Fig. 1. Schematic diagram of a graphene based liquid-gated FET biosensor with Au NPs decoration for DNA sensing in solution.

2.2. Gold nanoparticles decoration

Before attaching the PDMS wells, G-FET devices were decorated with Au NPs using a direct-current (DC) magnetron-sputtering inert-gas aggregation system (Fig. 2**a** [23,24,27–29]. A high purity (99 %) Au target was bombarded with an Ar plasma, freeing Au atoms for nanocluster formation in an initial chamber (aggregation zone). In this chamber, Au atoms nucleate into small clusters via collisions with Ar atoms and other Au atoms. Adjusting deposition parameters such as the plasma power and the pressure difference between the aggregation zone and deposition chamber, allowed us to control the nanoparticle size and crystallinity as they form from coalescing Au clusters. The aggregation zone is held at a higher pressure than the deposition chamber, forcing Au NPs to migrate into the deposition chamber and land on the target substrate. The particles also passed through a quadrupole mass filter (QMF) between the two chambers for size control. We selected Au NPs with an average diameter of 2.5 nm. The base pressure in the deposition chamber and aggregation zone before deposition was maintained below $\sim 1.5 \times 10^{-7}$ and $\sim 2.5 \times 10^{-6}$ mbar, whereas the process pressures were $\sim 1.4 \times 10^{-3}$ and $\sim 4.5 \times 10^{-1}$ mbar, respectively. Depositions were performed using an Ar flow rate of 100 sccm, a DC power of ~6 W and the length of the aggregation zone was 125 mm. The substrate holder was rotated at 2 rpm to ensure uniform NP decorating density. An AFM image of the Au NPs decorated graphene is shown in Fig. 2**b** After 1 h of deposition, the NPs density is approximately 5×10^{10} cm^{-2}, therefore each graphene device will present 5×10^8 binding sites to the biological solution.

2.3. Biological solution preparation

The dimeric form of the streptavidin-binding aptamer was derived from the monomeric form (StrepApt5) reported by Ruigrok VJ et al. [30]

Aptamer: 5′-thiol-modified/ AAAGGGAACGCACCGATCGCAGGTTTCCCATAAACACGACGCACCGATCGCAGGTTCGTG-3′ (60 nt)

Complementary strand (cDNA): 5′- TTTATGGGAAACCTGCGATCGGTGCGTTCCCTTT-3′ (34 nt)

SNP strand M1 (cDNA): 5′- TTTATGGGAAAGCTGCGATCGGTGCGTTCCCTTT-3′ (34 nt)

SNP strand M4 (cDNA): 5′- TTTATGGGAAACCTGCGATCGGTGCCTTCCCTTT-3′ (34 nt)

The disulfide in a thiol-modified aptamer solution was reduced to monothiol using tris (2-carboxyethyl) phosphine (TCEP 20 mM, 2 h at RT). A solution containing 1x TBE buffer (89 mM Tris, 89 mM boric acid, 2 mM EDTA, pH ~8.0), 1 μM TCEP, and 50 mM NaCl was used for cleaving the s-s bond of the 10 nM aptamer. This solution was kept at -20 °C. The following oligonucleotides were used for preparing 2000 bp DNA with 5′-thiol modification.

PCR primer 1: 5′-thiol-modifed/GTCTCGCGCGTTTCGGTGAT-3′ (20 nt)

PCR primer 2: GAACCGGAGCTGAATGAAGCC-3′ (21 nt)

The 2000 bp DNA with 5′-thiol modification was prepared by PCR

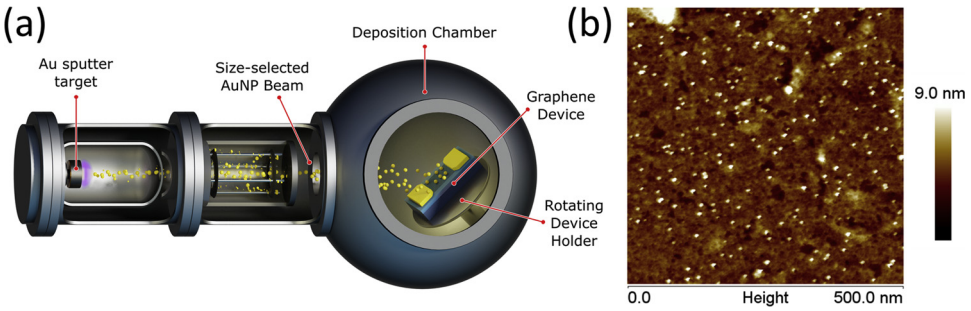

Fig. 2. (**a**) Schematic diagram of the magnetron sputtering inert gas condensing system for synthesis and size selection of the Au NPs. (**b**) AFM image of a graphene sheet decorated with Au NPs from the gas-phase synthesis method.

amplification of the pUC19 plasmid. The plasmid (10 ng) with primers 1 and 2 (0.5 μM each) were PCR amplified using 2 × Phusion Master Mix (New England Biolabs) in 25 μL reaction volume. After initial denaturation at 98 °C for 30 s, 25 cycles of 5 s at 98 °C followed by 45 s at 72 °C and 30 s at 70 °C were used. The resulting PCR product was column purified using a DNA Clean and Concentrator Kit (Zymo Research). A solution containing 3 nM of thiol-modified duplex DNA was subjected to TCEP treatment as mentioned previously. Streptavidin (10 nM) solution was prepared in 1x phosphate-buffered saline (PBS) buffer (137 mM NaCl, 2.7 mM KCl, 10 mM Na_2HPO_4, 1.8 mM KH_2PO_4, pH ~ 7.4).

2.4. Electrical measurements & characterization

Atomic force microscopy (AFM) was used to measure the Au NPs density on graphene devices. AFM topography measurements were performed on a conventional Multimode 8 scanning probe microscope (Bruker, USA) in PeakForce tapping mode. The high-resolution AFM probe (ScanAsyst-Air) from Bruker with nominal tip radius ~2 nm, resonant frequency 70 kHz, and low spring constant 0.4 N/m were used for all AFM measurements. The high resolution (512 by 512 pixels) AFM images were captured at a scan rate of 0.5 Hz and further processed by using the Nanoscope Analysis software (Ver 9).

The transfer characteristics of the liquid-gated G-FETs were measured using a semiconductor parameter analyzer (Keithley 4200-SCS-A) under a constant drain to source (V_{ds}) bias of 0.1 V. A silver wire (1 mm diameter) was used as the liquid gate electrode [10]. The DNA aptamer was bound to the Au NPs on the G-FET by placing a 40 μL drop of 10 μM DNA in buffer in the solution well overnight in a wet chamber at 4 °C. The device was rinsed with 1x PBS and DI water to remove unbound DNA strands. Before cDNA detection experiments, the graphene surface was passivated by incubating a 100 mM solution of ethanolamine in 0.01x PBS for 1 h at room temperature [11]. Before streptavidin detection experiments, BSA was used as a passivation layer instead by incubating with a 5 μM solution in DI water for 1 h. The schematic in Fig. 1 shows the reference electrode configuration and DNA bound to the Au NPs present during measurement.

3. Results

Graphene was grown on Cu foil using a CVD process and transferred to Si:SiO_2 substrates via a PVA lamination procedure described in Shivayogimath A et al. [16] This is a convenient, non-toxic, and scalable procedure that avoids etching or electrochemical delamination techniques. A typical microscope image of the resulting transferred graphene is shown in Fig. 3a, with small regions of darker purple color distributed over a lighter colored background. The darker zones, which suggest areas of thicker graphene [31], are arranged in a line style normal to the direction of laminate peeling. The linear arrangement is possible due to the stress accumulation during the peeling process, which indicates that the resulting device graphene thickness does not only depend on the CVD growth parameters, but also on the peeling procedure. Raman spectra acquired from these samples show two trends, seen in Fig. 3**b**. The top spectrum (black) was measured with the laser focus on the dark purple zone, while the bottom spectrum (red) was from the light background. In both spectra, four peaks were detected: D, G, D + D", and 2D modes. The G (ca. 1590 cm^{-1}) and 2D (ca. 2680 cm^{-1}) peaks are the typical Raman modes of graphene, from the first order in-plane vibration modes and second order in-plane transverse optical phonons, respectively. The D (1350 cm^{-1}) and D + D" (2450 cm^{-1}) peaks are mostly due to grain boundaries, surface contaminations, or other defects and strains formed during the transfer process. Both peaks are quite low and comparable to previous reports; indicating a low defect density in the transferred graphene [32–34].

It is well known that the 2D/G height ratio and the 2D peak symmetry can be used for estimating the thickness of graphene: a ratio of 2 for monolayer and 1 for bilayer graphene [35]. 2D/G peak height ratios were calculated to be 1.42 and 1.9 for the dark and light-colored zones, respectively. Deviation of the 2D/G ratio from the ideal value of 2.0 is due to the relatively large Raman laser spots, so that signals from both zones would inevitably be collected. The same theory also explains the value of 1.42 for the darker zones, as the height ratio should be ca. 1.0 for bilayer graphene. A Raman mapping image illustrating the 2D/G height ratio distribution is shown in Fig. 3c, in which regions of low ratio (blue) interspersed with regions of high 2 G/D (red). This observation from Raman mapping agrees with the optical microscope measurements that the laminate transferred graphene consists of an overall monolayer with isolated islands of bilayer graphene. Further optimization of the lamination or peeling procedure could suppress the formation of these regions, but large enough areas of monolayer graphene are present for ultrasensitive DNA detection via gas-phase synthesized Au NPs.

After patterning the monolayer graphene into an array of devices, Au NPs decoration was performed using a previously described magnetron sputtering inert gas condensing method [23,25]. The Au NPs were size selected to have an average diameter of 2.5 nm (Supplementary Fig. S1) using the QMF such that the DNA aptamer and the target analyte would bind within the Debye length of the liquid gate solution. At distances greater than this Debye length, the influence of charged biomolecules on the graphene is screened by adjusting counterions in the solution [9,36]. In this work, liquid gate measurements were carried out using a solution 0.01x PBS (pH 7.4) which has a Debye length of 7.2 nm. Fig. 2**b** shows the distribution of deposited Au NPs over an area of transferred graphene, which shows some variance in thickness due to the transfer procedure as described above.

Fig. 1 illustrates the working principle of the Au NPs decorated G-FET for DNA detection using transfer curve measurements. A silver wire immersed in the 0.0f1x PBS solution covering the graphene is used as a reference electrode to modulate the source to drain current via the electrostatic gating effect. This is shown in Supplementary Fig. S2a and b which illustrate the G-FET output and transfer characteristics, respectively. The I_d-V_d curve decreases with a slight reduction in

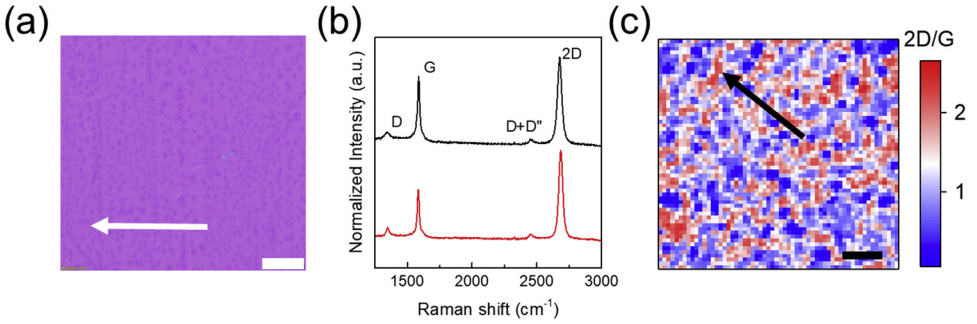

Fig. 3. (**a**) Microscope image of graphene on SiO_2/Si substrate. The scale is 10 μm and the arrow represents the peeling direction. (**b**) Typical Raman spectra of transferred graphene from the dark (black line) and light-colored (red line) zones in (a). (**c**) 2D/G peak height ratio of the transferred graphene from Raman mapping measurement. The scale bar is 5 μm and the arrow represents the peeling direction. (For interpretation of the references to colour in this figure legend, the reader is referred to the web version of this article).

magnitude of the applied liquid gate voltage, indicating the sensitivity of the device to the gate bias and verifying that a good ohmic contact exists between the graphene and gold electrode [37,38]. The G-FETs are operated at low voltages so that any electrochemical processes or gate currents are negligible; Fig. S2b shows that under normal G-FET operation, I_g is approximately 3 orders of magnitude smaller than I_d. Due to the electronic band structure of graphene, its conductivity cannot be switched off at room temperature. However, at some applied liquid gate voltage, the current will be at a minimum as the ambipolar device switches from the hole conducting regime to the electron conducting regime (moving from more negative to more positive voltages). This voltage is known as the charge neutrality potential, V_{CNP}, which can be affected by electrostatic gating or doping from molecules bound to the graphene. The shift in the V_{CNP} due to binding of a target analyte is the sensor response of the G-FET.

Fig. 4**a** shows the shift in transfer characteristics of the Au NPs decorated G-FET after DNA functionalization and ethanolamine passivation. Initially, the Au NPs decorated G-FET has a V_{CNP} of approximately 0.44 V, heavily p-doped from the ideal case of 0 V due to the p-type doping from the Au NPs deposition and adsorbates from the environment [11,39]. After exposure to a 10 μM solution of the thiol-terminated DNA aptamer, numerous single strands are strongly bound to the Au NPs via the Au-S bond. This causes a large leftward, negative shift in the V_{CNP} to approximately 0.3 V as the electron-rich nucleobases in the DNA n-dope the graphene. Electrostatic gating from the negatively charged bound DNA aptamer would instead result in a positive shift, therefore our results can more easily be explained by n-doping of the graphene channel from interactions between the DNA backbone and the graphene surface [4]. From the method described by Xu et al. 2017, we estimate the density of bound aptamers on the G-FET to be $3.5 \times 10^{10}\,cm^{-2}$, comparable to the density of deposited Au NPs seen in the AFM imaging experiments [40]. This leftward shift in response to DNA binding is commonly seen in G-FETs that utilize Au NPs [4,10,11,39], in contrast to chemically functionalized G-FETs which report a positive V_{CNP} shift from DNA binding due to electrostatic gating [9,12]. The G-FET is then passivated using an ethanolamine solution to deactivate and block reactive groups on the graphene surface, preventing non-specific binding.

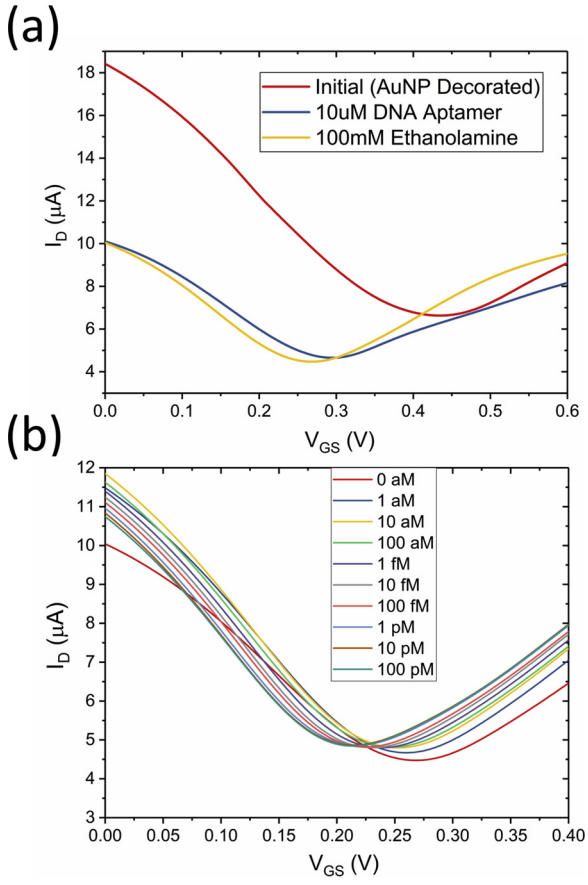

Fig. 4. (**a**) Characteristic G-FET transfer curves at each functionalization step. (**b**) Characteristic G-FET transfer curves after hybridization with different concentrations of the complementary strand (cDNA) to the DNA aptamer.

After the passivation step, we performed the DNA sensing experiments. Beginning with the lowest concentration, a droplet of buffered DNA fully complementary to the aptamer (cDNA) was placed on the G-FET channel and interacted with the Au NPs bound aptamer for 30 min to allow hybridization [11,12,15,41]. Afterwards, the device was rinsed with 1X PBS and DI water to remove weakly bound or unhybridized strands, and the transfer characteristics were measured again in 0.01x PBS. Fig. 4**b** shows the set of G-FET transfer curves for different concentrations of cDNA from 1 aM to 100 pM. As the cDNA concentration increases, a steady leftwards shift in V_{CNP} is observed, indicating increasing n-doping of the graphene channel by the cDNA. For cDNA concentrations greater than 1 pM, V_{CNP} does not significantly change, as the DNA aptamer strands bound to the Au NPs have all been hybridized and no further doping is possible. The slight increase in minimum current with increased cDNA concentration can be explained with charge doping and the interaction of the charged molecules with charged impurities on the graphene surface [7,42]. Due to doping from the cDNA, electron density in the graphene channel increases, resulting in an upward shift of the Fermi level. Electron mobility is preserved due to increased scattering of hole carriers in the graphene channel with the negatively charged cDNA [7]. Positively charged impurities in the graphene channel or defects are screened by counterions in the solution [43,44].

Fig. 5 shows the shift in the charge neutrality point (ΔV_{CNP}) for two series of measurements on Au NPs decorated and bare G-FET devices exposed to cDNA concentrations of 1 aM to 100 pM. Each data point in Fig. 5 is an average of 5 different G-FETs and the error bars are one standard deviation. The Au NP functionalized sensor exhibits a log-linear response between 1 aM and 1 pM before saturating at $\Delta V_{CNP} \approx 50$ mV in the picomolar cDNA concentration range. This corresponds to a sensitivity to six orders of magnitude in analyte concentration, or a

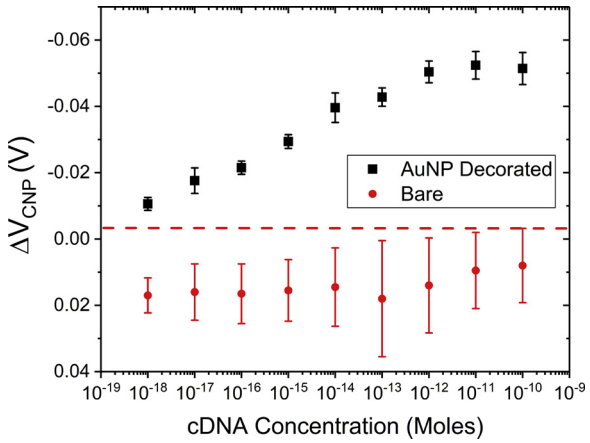

Fig. 5. The shift of V_{CNP} for Au NPs decorated (black squares) and bare (red circles) G-FET biosensors after exposure to a series of concentrations (from 1 aM to 100 pM) of DNA fully complementary to the aptamer. Error bars indicate standard deviations from measurements with five different devices and the dotted line indicates the maximum response of the undecorated G-FET to the cDNA solutions. (For interpretation of the references to colour in this figure legend, the reader is referred to the web version of this article).

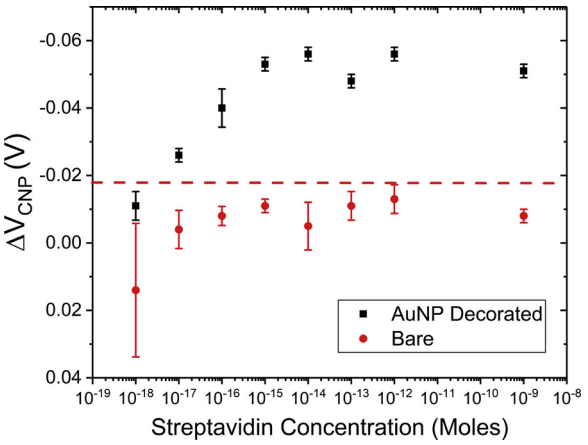

Fig. 7. The shift of V_{CNP} for Au NPs decorated (black squares) and bare (red circles) G-FET biosensors after exposure to a series of concentrations (from 1 aM to 1 nM) of streptavidin in 0.01xPBS. Error bars indicate standard deviations from measurements with five different devices and the dotted line indicates the maximum response of the undecorated G-FET to the streptavidin solutions. (For interpretation of the references to colour in this figure legend, the reader is referred to the web version of this article).

dynamic range of 10^6. In contrast, the bare G-FETs do not exhibit any consistent leftward shift in V_{CNP} and remain stable at a slight positive shift relative to the passivation step. In the dynamic range of this biosensor, a sensitivity of approximately 8 mV/decade is achieved, which is 2–3 times lower than the best results reported in the literature [45]. This may be due to the less DNA aptamer binding sites presented after Au NPs decoration (roughly 10^{10} cm^{-2}), compared to other chemical functionalization methods which normally result in DNA probe densities of 10^{13} cm^{-2} [12]. Extending the Au NPs deposition time or changing the width/length (W/L) ratio of the G-FETs should further enhance the sensitivity.

The specificity of the sensor was tested by comparing the ΔV_{CNP} upon exposure to 100 pM of the cDNA, and two different sequences which each exhibit a different single nucleotide polymorphism (M1 and M4 SNP). In Fig. 6, it is apparent that the one-base mismatched SNP exhibit a significantly reduced ΔV_{CNP} at 100 pM, roughly equivalent to the shift produced by the fully complementary strand at 1 aM (~ 10 mV). This shift in ΔV_{CNP} is also similar in magnitude to the shift seen in G-FET hysteresis and extended bias stress measurements (Supplementary Fig. S2c and d), which is due to carrier density enhancement in the graphene caused by capacitive gating [46]. We can use the maximum signal produced by the M1 SNP to set the limit of detection (LoD) of the sensor to ≈ 15 aM, a significant improvement over many G-FETs functionalized by chemical methods or solvent-based Au NPs [10–12,45,47]. The achieved LoD indicates that using graphene transferred via the laminate method does not intrinsically limit the sensitivity of biosensor G-FETs.

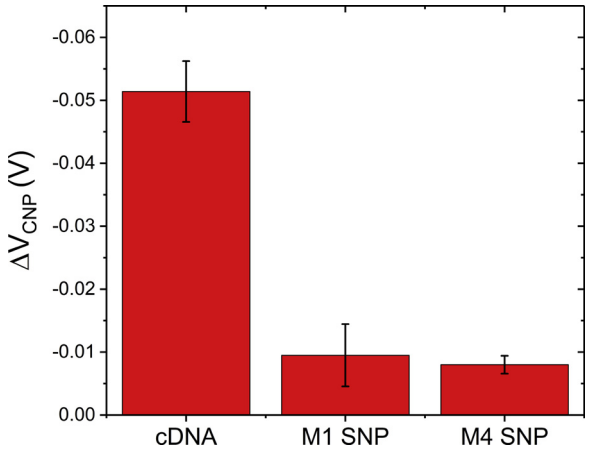

Fig. 6. The shift of V_{CNP} for Au NPs decorated G-FET devices after exposure to 100 pM of DNA fully complementary to the aptamer (cDNA) and to two different sequences with single nucleotide polymorphisms (M1 and M4 SNP).

We can also employ the G-FETs functionalized with the DNA aptamer to sense streptavidin in a 0.01x PBS solution. After passivation with 5 μM of BSA, solutions of streptavidin in 0.01x PBS were placed on the G-FET channel and left to interact with the DNA aptamer bound to the Au NPs. The transfer characteristics of the devices were measured after 30 min. without an intervening rinsing step, to prevent the weakly bound streptavidin from being detached from the DNA aptamer. Fig. 7 shows the ΔV_{CNP} for two series of measurements on Au NPs decorated and bare G-FET devices exposed to streptavidin concentrations of 1 aM to 100 pM. As before, each data point in Fig. 7 is an average of 5 different G-FETs and the error bars are one standard deviation. Streptavidin is known to have a slight negative charge in neutral pH solutions [48,49], therefore a leftward shift due to the n-doping of graphene that increases with solution concentration is again observed. As for the cDNA case, the G-FET sensor is capable of analyte detection in the attomolar range, using the maximum response of the bare graphene sensor to the streptavidin solutions as the noise limit for the sensor. We estimate an LoD of ≈ 9 aM and a sensitivity of approximately 14 mV/decade. However, the G-FET rapidly saturates upon exposure to 1 fM concentrations of streptavidin (dynamic range of 10^3) and is less stable at higher concentrations. Due to streptavidin's much lower charge in solution than the complementary strand [49], a higher population of binding sites may be required to improve this dynamic range.

4. Conclusion

In summary, we have developed an Au NPs-decorated graphene FET biosensor capable of label-free and ultrasensitive (in the attomolar range) detection of DNA and streptavidin using a liquid gate measurement. The sensor was fabricated using a simple graphene lamination method and functionalized via solvent-free gas-phase synthesized Au NPs, a novel combination. Undecorated G-FETs show no sensor response to the complementary DNA strand or streptavidin. The decorated G-FET can detect full hybridization of the complementary strand down to 15 aM; solutions with SNP-containing DNA only produce an equivalent response at concentrations 7 orders of magnitude higher.

CRediT authorship contribution statement

Eric Danielson: Conceptualization, Methodology, Investigation, Writing - original draft. **Vyankat A. Sontakke:** Resources. **Alexander J. Porkovich:** Resources, Investigation, Writing - review & editing. **Zhenwei Wang:** Methodology, Investigation, Writing - review & editing. **Pawan Kumar:** Investigation. **Zakaria Ziadi:** Methodology, Writing - review & editing. **Yohei Yokobayashi:** Conceptualization, Supervision, Project administration. **Mukhles Sowwan:** Conceptualization, Supervision, Project administration.

Declaration of Competing Interest

The authors declare no competing financial interest.

Acknowledgements

This work was supported by funding from the Okinawa Institute of Science and Technology Graduate University (OIST). Device fabrication was carried out at OIST under the supervision of the Engineering Support Section; the authors are particularly thankful for the help of Alexander Badrutinov. We are also grateful for data visualization help provided by Pavel Puchenkov from the Data Analysis Section of the Research Support division at OIST.

Appendix A. Supplementary data

Supplementary material related to this article can be found, in the online version, at doi:https://doi.org/10.1016/j.snb.2020.128432.

References

[1] M. Pumera, Graphene in biosensing, Mater. Today 14 (7) (2011) 308–315.
[2] K. Matsumoto, K. Maehashi, Y. Ohno, K. Inoue, Recent advances in functional graphene biosensors, J. Phys. D Appl. Phys. 47 (9) (2014) 094005.
[3] S. Viswanathan, T.N. Narayanan, K. Aran, K.D. Fink, J. Paredes, P.M. Ajayan, S. Filipek, P. Miszta, H.C. Tekin, F. Inci, U. Demirci, P. Li, K.I. Bolotin, D. Liepmann, V. Renugopalakrishanan, Graphene–protein field effect biosensors: glucose sensing, Mater. Today 18 (9) (2015) 513–522.
[4] C. Andronescu, W. Schuhmann, Graphene-based field effect transistors as biosensors, Curr. Opin. Electrochem. 3 (1) (2017) 11–17.
[5] P. Suvarnaphaet, S. Pechprasarn, Graphene-based materials for biosensors: a review, Sensors 17 (10) (2017).
[6] S.D. Jayasena, Aptamers: an emerging class of molecules that rival antibodies in diagnostics, Clin. Chem. 45 (9) (1999) 1628.
[7] D.-J. Kim, H.-C. Park, I.Y. Sohn, J.-H. Jung, O.J. Yoon, J.-S. Park, M.-Y. Yoon, N.-E. Lee, Electrical graphene aptasensor for ultra-sensitive detection of anthrax toxin with amplified signal transduction, Small 9 (19) (2013) 3352–3360.
[8] M. Kaisti, Detection principles of biological and chemical FET sensors, Biosens. Bioelectron. 98 (2017) 437–448.
[9] W. Fu, L. Jiang, E.P. van Geest, L.M.C. Lima, G.F. Schneider, Sensing at the surface of graphene field-effect transistors, Adv. Mater. 29 (6) (2017) 1603610.
[10] T.-Y. Chen, P.T.K. Loan, C.-L. Hsu, Y.-H. Lee, J. Tse-Wei Wang, K.-H. Wei, C.-T. Lin, L.-J. Li, Label-free detection of DNA hybridization using transistors based on CVD grown graphene, Biosens. Bioelectron. 41 (2013) 103–109.
[11] B. Cai, L. Huang, H. Zhang, Z. Sun, Z. Zhang, G.-J. Zhang, Gold nanoparticles-decorated graphene field-effect transistor biosensor for femtomolar MicroRNA detection, Biosens. Bioelectron. 74 (2015) 329–334.
[12] R. Campos, J. Borme, J.R. Guerreiro, G. Machado Jr., M.F. Cerqueira, D.Y. Petrovykh, P. Alpuim, Attomolar label-free detection of DNA hybridization with electrolyte-gated graphene field-effect transistors, ACS Sens. 4 (2) (2019) 286–293.
[13] Y. Yang, A.M. Asiri, Z. Tang, D. Du, Y. Lin, Graphene based materials for biomedical applications, Mater. Today 16 (10) (2013) 365–373.
[14] G. Saltzgaber, P.M. Wojcik, T. Sharf, M.R. Leyden, J.L. Wardini, C.A. Heist, A.A. Adenuga, V.T. Remcho, E.D. Minot, Scalable graphene field-effect sensors for specific protein detection, Nanotechnology 24 (35) (2013) 355502.
[15] A.A. Saeed, J.L.A. Sánchez, C.K. O'Sullivan, M.N. Abbas, DNA biosensors based on gold nanoparticles-modified graphene oxide for the detection of breast cancer biomarkers for early diagnosis, Bioelectrochemistry 118 (2017) 91–99.
[16] A. Shivayogimath, P.R. Whelan, D.M.A. Mackenzie, B. Luo, D. Huang, D. Luo, M. Wang, L. Gammelgaard, H. Shi, R.S. Ruoff, P. Bøggild, T.J. Booth, Do-it-yourself transfer of large-area graphene using an office laminator and water, Chem. Mater. 31 (7) (2019) 2328–2336.
[17] M.B. Lerner, D. Pan, Y. Gao, L.E. Locascio, K.-Y. Lee, J. Nokes, S. Afsahi, J.D. Lerner, A. Walker, P.G. Collins, K. Oegema, F. Barron, B.R. Goldsmith, Large scale commercial fabrication of high quality graphene-based assays for biomolecule detection, Sens. Actuators B Chem. 239 (2017) 1261–1267.
[18] J. Wang, A. Shi, X. Fang, X. Han, Y. Zhang, An ultrasensitive supersandwich electrochemical DNA biosensor based on gold nanoparticles decorated reduced graphene oxide, Anal. Biochem. 469 (2015) 71–75.
[19] H. Song, X. Li, P. Cui, S. Guo, W. Liu, X. Wang, Morphology optimization of CVD graphene decorated with Ag nanoparticles as ammonia sensor, Sens. Actuators B Chem. 244 (2017) 124–130.
[20] N.M. Galdino, G.S. Brehm, R. Bussamara, W.D.G. Gonçalves, G. Abarca, J.D. Scholten, Sputtering deposition of gold nanoparticles onto graphene oxide functionalized with ionic liquids: biosensor materials for cholesterol detection, J. Mater. Chem. B 5 (48) (2017) 9482–9486.
[21] G.E. Johnson, R. Colby, J. Laskin, Soft landing of bare nanoparticles with controlled size, composition, and morphology, Nanoscale 7 (8) (2015) 3491–3503.
[22] R.E. Palmer, R. Cai, J. Vernieres, Synthesis without solvents: the cluster (nanoparticle) beam route to catalysts and sensors, Acc. Chem. Res. 51 (9) (2018) 2296–2304.
[23] S. Steinhauer, V. Singh, C. Cassidy, C. Gspan, W. Grogger, M. Sowwan, A. Köck, Single CuO nanowires decorated with size-selected Pd nanoparticles for CO sensing in humid atmosphere, Nanotechnology 26 (17) (2015) 175502.
[24] P. Grammatikopoulos, S. Steinhauer, J. Vernieres, V. Singh, M. Sowwan, Nanoparticle design by gas-phase synthesis, Adv. Phys. X 1 (1) (2016) 81–100.
[25] E. Danielson, V. Dhamodharan, A. Porkovich, P. Kumar, N. Jian, Z. Ziadi, P. Grammatikopoulos, V.A. Sontakke, Y. Yokobayashi, M. Sowwan, Gas-phase synthesis for label-free biosensors: zinc-oxide nanowires functionalized with gold nanoparticles, Sci. Rep. 9 (1) (2019) 17370.
[26] R. Wu, L. Gan, X. Ou, Q. Zhang, Z. Luo, Detaching graphene from copper substrate by oxidation-assisted water intercalation, Carbon 98 (2016) 138–143.
[27] J. Vernieres, S. Steinhauer, J. Zhao, P. Grammatikopoulos, R. Ferrando, K. Nordlund, F. Djurabekova, M. Sowwan, Site-specific wetting of Iron nanocubes by gold atoms in gas-phase synthesis, Adv. Sci. 6 (13) (2019) 1900447.
[28] A.J. Porkovich, Z. Ziadi, P. Kumar, J. Kioseoglou, N. Jian, L. Weng, S. Steinhauer, J. Vernieres, P. Grammatikopoulos, M. Sowwan, In situ observation of metal to metal oxide progression: a study of charge transfer phenomenon at Ru-CuO interface, ACS Nano 13 (2019) 12425–12437.
[29] A. Datta, A.J. Porkovich, P. Kumar, G. Nikoulis, J. Kioseoglou, T. Sasaki, S. Steinhauer, P. Grammatikopoulos, M. Sowwan, Single nanoparticle activities in ensemble: a study on Pd cluster nanoportals for electrochemical oxygen evolution reaction, J. Phys. Chem. C 123 (43) (2019) 26124–26135.
[30] V.J.B. Ruigrok, E. van Duijn, A. Barendregt, K. Dyer, J.A. Tainer, R. Stoltenburg, B. Strehlitz, M. Levisson, H. Smidt, J. van der Oost, Kinetic and stoichiometric characterisation of streptavidin-binding aptamers, ChemBioChem 13 (6) (2012) 829–836.
[31] Y.-S. No, H.K. Choi, J.-S. Kim, H. Kim, Y.-J. Yu, C.-G. Choi, J.S. Choi, Layer number identification of CVD-grown multilayer graphene using Si peak analysis, Sci. Rep. 8 (1) (2018) 571.
[32] S. Roscher, R. Hoffmann, O. Ambacher, Determination of the graphene–graphite ratio of graphene powder by Raman 2D band symmetry analysis, Anal. Methods 11 (9) (2019) 1224–1228.
[33] S. Afsahi, M.B. Lerner, J.M. Goldstein, J. Lee, X. Tang, D.A. Bagarozzi, D. Pan, L. Locascio, A. Walker, F. Barron, B.R. Goldsmith, Novel graphene-based biosensor for early detection of Zika virus infection, Biosens. Bioelectron. 100 (2018) 85–88.
[34] R. Campos, G. Machado, M.F. Cerqueira, J. Borme, P. Alpuim, Wafer scale fabrication of graphene microelectrode arrays for the detection of DNA hybridization, Microelectron. Eng. 189 (2018) 85–90.
[35] D. Graf, F. Molitor, K. Ensslin, C. Stampfer, A. Jungen, C. Hierold, L. Wirtz, Spatially resolved raman spectroscopy of single- and few-layer graphene, Nano Lett. 7 (2) (2007) 238–242.
[36] E. Stern, R. Wagner, F.J. Sigworth, R. Breaker, T.M. Fahmy, M.A. Reed, Importance of the debye screening length on nanowire field effect transistor sensors, Nano Lett. 7 (11) (2007) 3405–3409.
[37] L. Zhou, K. Wang, H. Sun, S. Zhao, X. Chen, D. Qian, H. Mao, J. Zhao, Novel graphene biosensor based on the functionalization of multifunctional nano-bovine serum albumin for the highly sensitive detection of cancer biomarkers, Nano-Micro Lett. 11 (1) (2019).
[38] S. Chen, Y. Sun, Y. Xia, K. Lv, B. Man, C. Yang, Donor effect dominated molybdenum disulfide/graphene nanostructure-based field-effect transistor for ultrasensitive DNA detection, Biosens. Bioelectron. 156 (2020) 112128.
[39] X. Dong, Y. Shi, W. Huang, P. Chen, L.-J. Li, Electrical detection of DNA hybridization with single-base specificity using transistors based on CVD-grown graphene sheets, Adv. Mater. 22 (14) (2010) 1649–1653.
[40] S. Xu, J. Zhan, B. Man, S. Jiang, W. Yue, S. Gao, C. Guo, H. Liu, Z. Li, J. Wang, Y. Zhou, Real-time reliable determination of binding kinetics of DNA hybridization using a multi-channel graphene biosensor, Nat. Commun. 8 (2017) 14902.
[41] A. Shi, J. Wang, X. Han, X. Fang, Y. Zhang, A sensitive electrochemical DNA biosensor based on gold nanomaterial and graphene amplified signal, Sens. Actuators B Chem. 200 (2014) 206–212.
[42] D.-J. Kim, I.Y. Sohn, J.-H. Jung, O.J. Yoon, N.E. Lee, J.-S. Park, Reduced graphene oxide field-effect transistor for label-free femtomolar protein detection, Biosens. Bioelectron. 41 (2013) 621–626.
[43] F. Chen, Q. Qing, J. Xia, J. Li, N. Tao, Electrochemical gate-controlled charge transport in graphene in ionic liquid and aqueous solution, J. Am. Chem. Soc. 131 (29) (2009) 9908–9909.
[44] F. Chen, J. Xia, N. Tao, Ionic screening of charged-impurity scattering in graphene, Nano Lett. 9 (4) (2009) 1621–1625.

[45] S. Xu, S. Jiang, C. Zhang, W. Yue, Y. Zou, G. Wang, H. Liu, X. Zhang, M. Li, Z. Zhu, J. Wang, Ultrasensitive label-free detection of DNA hybridization by sapphire-based graphene field-effect transistor biosensor, Appl. Surf. Sci. 427 (2018) 1114–1119.
[46] H. Wang, Y. Wu, C. Cong, J. Shang, T. Yu, Hysteresis of electronic transport in graphene transistors, ACS Nano 4 (12) (2010) 7221–7228.
[47] B. Cai, S. Wang, L. Huang, Y. Ning, Z. Zhang, G.-J. Zhang, Ultrasensitive label-free detection of PNA–DNA hybridization by reduced graphene oxide field-effect transistor biosensor, ACS Nano 8 (3) (2014) 2632–2638.
[48] B.M. Lowe, K. Sun, I. Zeimpekis, C.-K. Skylaris, N.G. Green, Field-effect sensors – from pH sensing to biosensing: sensitivity enhancement using streptavidin–biotin as a model system, Analyst 142 (22) (2017) 4173–4200.
[49] S. Sivasankar, S. Subramaniam, D. Leckband, Direct molecular level measurements of the electrostatic properties of a protein surface, Proc. Natl. Acad. Sci. 95 (1998) 12961–12966.

Eric Danielson received his Ph.D. from the University of Texas at Austin in 2014. His research interest focuses on FET biosensors.

Vyankat A. Sontakke received his Ph.D. from Savitribai Phule Pune University in 2015. His research interest focuses on the synthesis of some antiviral benzimidazole nucleosides and their analogues.

Alexander J. Porkovich received his Ph.D. from the University of Technology in Sydney in 2013. His research interest focuses on the gas-phase synthesis of nanoparticles for catalysis applications.

Zhenwei Wang received his Ph.D. from King Abdullah University of Science and Technology in 2018. His research interest focuses on thin film transistors and low dimensional materials.

Pawan Kumar received his Ph.D. from Jaypee University of Information Technology in 2015. His research focuses on the understanding of electronic transport behavior of nanoparticle-decorated semiconducting nanowire devices using scanning probe microscopy.

Zakaria Ziadi received his Ph.D. from the University of the Ryukyus in 2015. His research interest focuses on the effect of gas phase synthesized nanoparticles on semiconducting nanowire-based micro devices and their applicability in gas sensing, bio sensing and battery applications.

Yohei Yokobayashi received his Ph.D. from the Scripps Research Institute in 2001. He is currently the head of the Nucleic Acid Chemistry and Engineering Unit at the Okinawa Institute of Science and Technology.

Mukhles Sowwan is the director of the Nanoparticles by Design Unit at Okinawa Institute of Science and Technology (OIST)-Japan and a visiting professor at SLAC national laboratory-CA-USA. His research is focused on the design and fabrication of multifunctional -multicomponent Nanoparticles for Nanotechnology and Bio-medical Applications.